Article

On the Seasonal Variations of the Bering Slope Current

Humio MITSUDERA[1], Youichi HIRANO[2], Hatsumi NISHIKAWA[3] and Hung Wei SHU[4]

[1] Institute of Low Temperature Sciences, Hokkaido University, Sapporo, Japan
[2] Graduate School of Environmental Science, Hokkaido University, Sapporo, Japan
[3] Atmosphere and Ocean Research Institute, University of Tokyo, Kashiwa, Japan
[4] Japan Fisheries Research and Education Agency, Kushiro, Japan

Abstract

Seasonal variations of the Bering Slope Current (BSC) and eddies were discussed by analyzing an ocean general circulation model output. The model simulates the seasonal variations of the BSC realistically, in which the BSC flows along the shelf break over the slope in winter, and moves off-slope during spring and summer. Eddies start growing in winter, resulting in the BSC's separation from the shelf-break. The eddies grow as a result of baroclinic instability owing to the deepening of the main pycnocline of the BSC in winter, which is likely to be affected remotely by the deepening of the Alaskan Stream in the Gulf of Alaska.

Key words: Bering Slope Current, eddies, baroclinic instability

1. Introduction

The Bering Sea located between Siberia and Alaska. While the northeast portion of the sea is a wide and shallow continental shelf, its deep portion of the sea is divided into three connected deep basins and the largest one is the Aleutian Basin (Fig. 1 upper panel). The Bering Slope Current (BSC) flows over a steep slope that connects the continental shelf and the deep basin (Fig. 1 lower panel). The BSC is known as the Green Belt where the biological production is active throughout the year (Springer *et al.*, 1996). It was suggested that the high biological production would be supported by mixing along the BSC between nutrients originating in the deep basin and iron from sediments over the shallow continental shelf due to tidal mixing and eddies (*e.g.* Tanaka *et al.*, 2017).

The BSC exhibits distinct seasonal variations observed by satellite altimetry (Ladd, 2012). During winter, the BSC is strong and tightly confined to the continental slope. The BSC starts broadening and moves off-slope during spring and reaches the deep basin in summer. It appears that anticyclonic eddies drive the evolution of the BSC; the eddies grow during spring when the BSC moves off slope, and are matured in summer when the BSC reaches the deep basin (Ladd, 2014; Okkonen, 2001; Mizobata *et al.*, 2002). These anticyclonic eddy generation is likely associated with shelf-break canyons called Navarin Canyon, Zhemchug Canyon, and Pribilof Canyon (Fig. 1 lower panel). However, it is not known why the BSC exhibits such a distinct seasonality as described above and its relationship with eddies. Specifically, the questions are:

- Why does the BSC move from the slope into the deep basin during spring?
- How do eddies form and grow? What are roles of eddies in the BSC evolution?
- What are the energy sources of the seasonal evolution of the BSC?

We addressed these questions by analyzing an ocean model output by Matsuda *et al.* (2015).

2. Data

The model output by Matsuda *et al.* (2015), based on an ice-coupled ocean general circulation model (OGCM) developed at the Atmosphere and Ocean Research Institute, the University of Tokyo, was used to analyze the BSC. The horizontal coordinates is finer than 3km in the northwestern continental shelf in the Sea of Okhotsk, while it becomes approximately 10 km in the Bering Sea (Matsuda *et al.*, 2015). Vertically 7 sigma coordinate grids were arranged shallower than 35m, under which 77 level coordinates are assigned. This model adopts the turbulence closure scheme (Noh and Kim 1999) to simulate the evolution of the oceanic surface and bottom boundary layers. Ocean and sea ice were driven by atmospheric forcing calculated from Ocean Model Intercomparison Project (OMIP) Ver. 6. The tidal forcing of the K1 is applied to the momentum equation. Readers may find detailed information on the model in Matsuda *et al.* (2015).
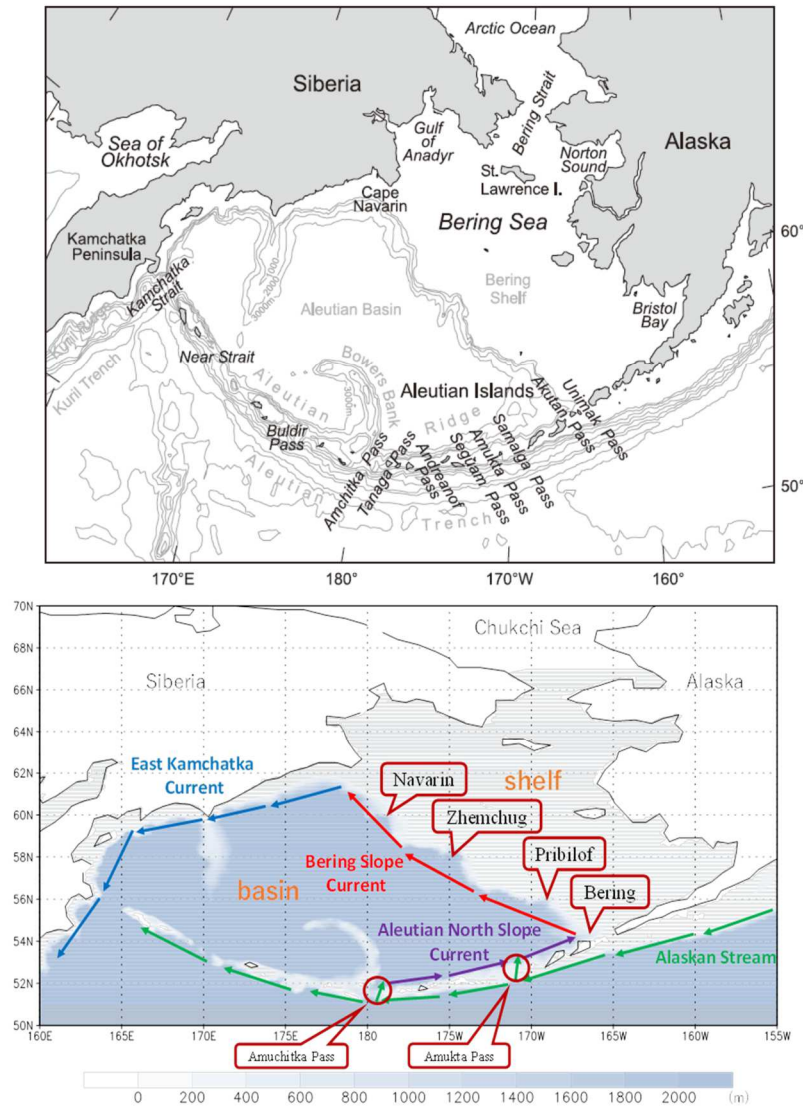
Fig. 1 (Upper) Geography of the Bering Sea (adopted from Foreman *et al*., 2006). (Lower) Location of the Bering Slope Current and key geographical names in this study. Grey shade denotes the ocean depth.

3. Overview of modeling results

Figure 2 displays a seasonal march of the surface current of the BSC reproduced in the model. The seasonal march of the model well represents variations observed by satellite (Ladd, 2012, 2014). The BSC is the strongest in winter (January to March). It flows over the slope adjacent to the shelf break. The BSC starts separating from the slope, with weakening its strength (April-June). Then, the BSC reaches the deep basin, although the mean current field becomes relatively weak compared with the BSC's amplitude of other seasons. In summer (July-September) the BSC is located at approximately 3 degrees away from the slope. Then, a new BSC starts forming along the slope in fall (October-December).

This seasonal march resembles closely to the BSC's seasonality in reality (Ladd, 2012). The off-slope speed of the BSC axis propagation (depicted by the meridional surface current) along an observation line off the Zhemchug Canyon is approximately 0.013 m s^{-1} from February to July (Fig. 3), consistent with satellite observations (Okkonen, 2001). This off-slope propagation of the BSC is likely associated with the growth of clockwise eddies along the slope during spring to early summer. Figure 4 displays isopycnal depth anomaly from the annual mean on the 27.0 σ_θ, in which we can find anticlockwise eddies' development along the slope. We also find a current reversal in Fig. 3 that develops from April until October, indicating that a stationary eddy forms over the continental slope off the Zhemchug Canyon. Similar eddy development is found off the Pribilof Canyon and Navarin Canyon as well.
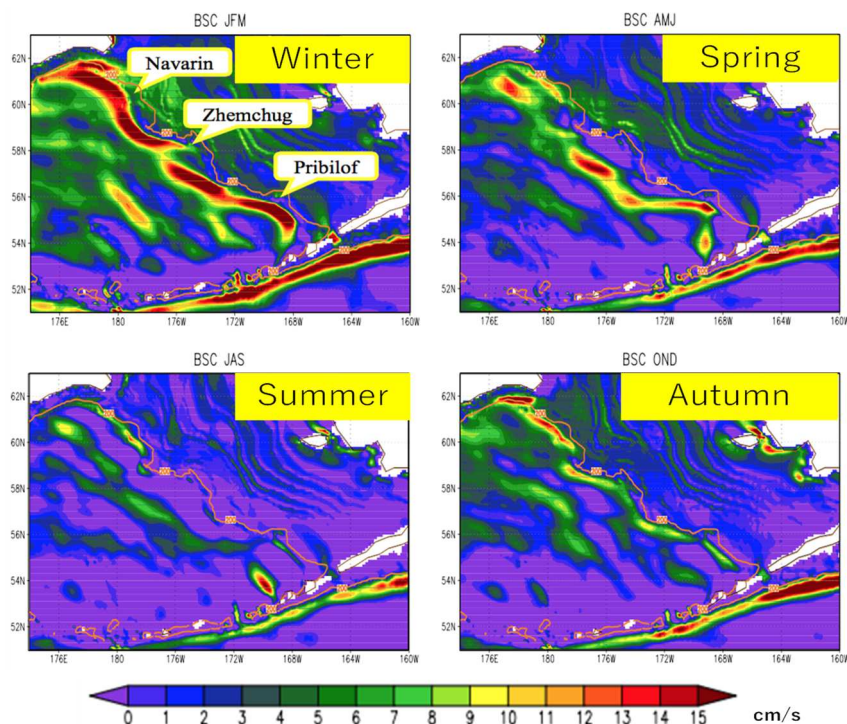
Fig. 2. Seasonal mean of the surface current speed along the shelf break in the Bering Sea. Seasonal evolution of the BSC is shown.
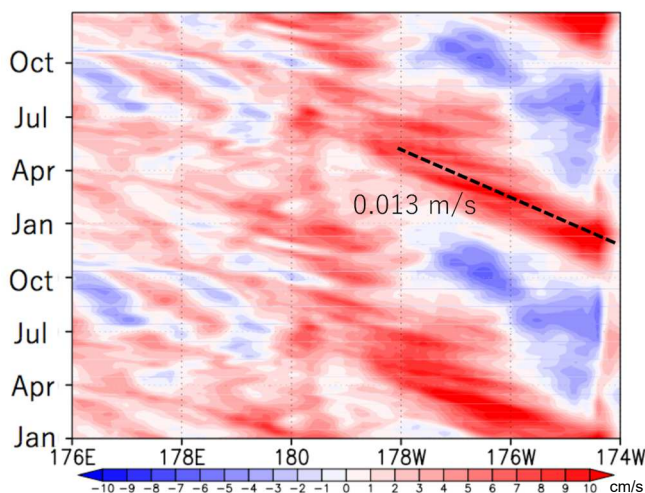

Fig. 3 Hovmöller diagram representing the meridional surface current off the Zhemchug Canyon along 57.5°N. Reddish (bluish) color denotes northward (southward) current (with a unit of cm/s). Dashed line denotes the propagation speed of the BSC axis in the offslope direction.

Figure 4 indicates that during winter, a positive depth anomaly as large as ~40 m is present over the slope confined to the shelf break, while a negative anomaly of ~ -40 m exists off-slope. This corresponds to a steep inclination of the pycnocline, *i.e.* the pycnocline front, where the BSC flows in February. The area of the positive depth anomaly broadens during spring and summer, resulting in the pycnocline deepening away from the slope. The negative anomaly ahead of the positive anomaly propagates westward as well, keeping a steep pycnocline front in-between. On the other hand, a substantial shoaling appears along the shelf break during summer and it broadens westward in fall.

A vertical section of the velocity and density field along 57.5°N reveals that the BSC has a baroclinic jet structure in which the isopycnals of 26.8-27.4 σ_θ incline toward the slope during autumn and winter (Fig. 5). In November, the BSC emerges approximately at 175°W tightly confined to the shelf break with the inclination of the isopycnals toward the slope. The BSC broadens to 176°W in February keeping the baroclinic jet structure. The current is quite deep. It flows northward with a speed as high as 0.03 ms^{-1} at a depth of 1000m, which is consistent with observations by Argo floats (Johnson *et al.*, 2004). Nevertheless, a southward flow can be observed below 600 m immediately adjacent to the slope. In May, the BSC start separating from the shelf break, developing a current reversal in the in-slope side. The BSC moves into the deep basin completely in August. The isopycnals exhibit a bowl shape between 174°W and 179°W, indicating the presence of a stationary anticyclonic eddy. The BSC is recognized as a northward current at 179°W along the limb of the stationary eddy. The BSC's vertical extent is shallower than the BSC in winter.

Anticyclonic eddies with a diameter of 200 km are prominent in a snapshot flow field, consistent with satellite observations (Ladd, 2012). The horizontal scale of eddies is closely related to the scale of the canyons.

As described above, the present model simulates the BSC well. Therefore, the model output was utilized to analyze the seasonality of the BSC and associated eddies.
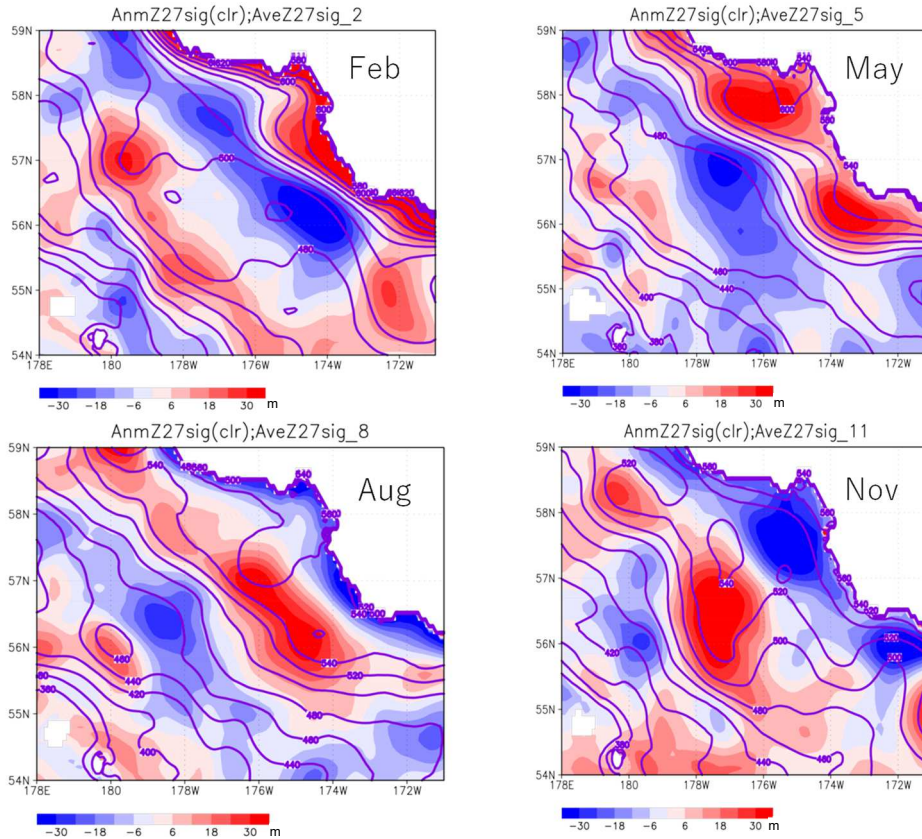
Fig. 4 Color shade depicts sopycnal depth anomaly of 27.0 σ_θ with a unit of m from February to November off the Zhemchug Canyon. Reddish color denotes deepening, while bluish color denotes shoaling. Contours denote depths of the 27.0 σ_θ with the contour interval of 20 m.

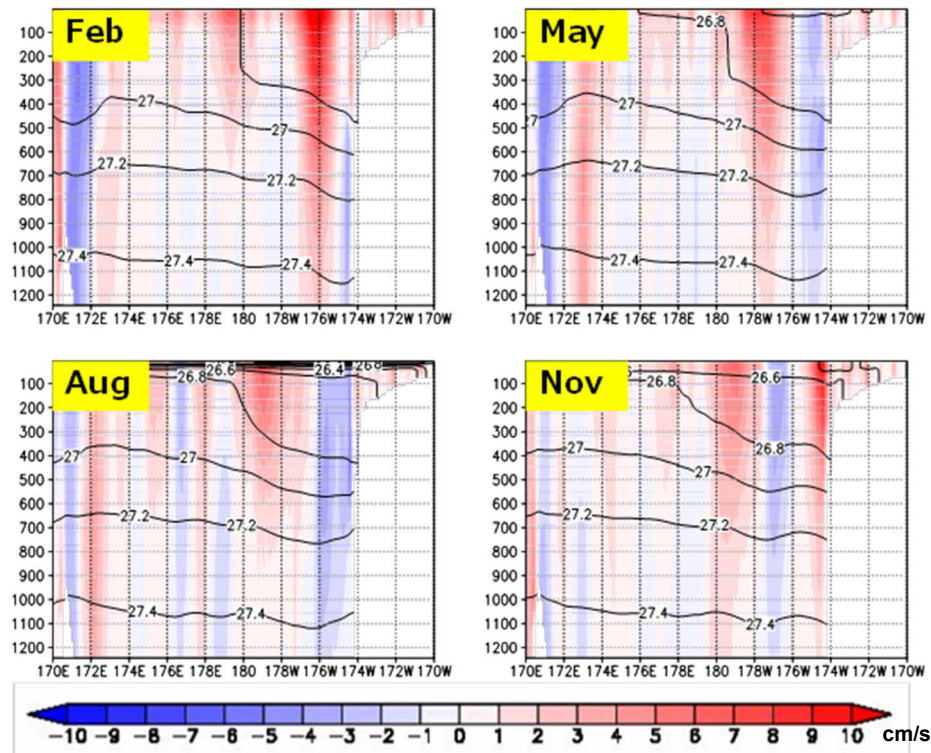Fig. 5 Vertical sections of meridional current (color shade) and density (contours) on the 57.5°N off the Zhemchug Canyon. Reddish (bluish) color denotes northward (southward) current with a unit of cm/s. Contour interval is 0.2 σ_θ.
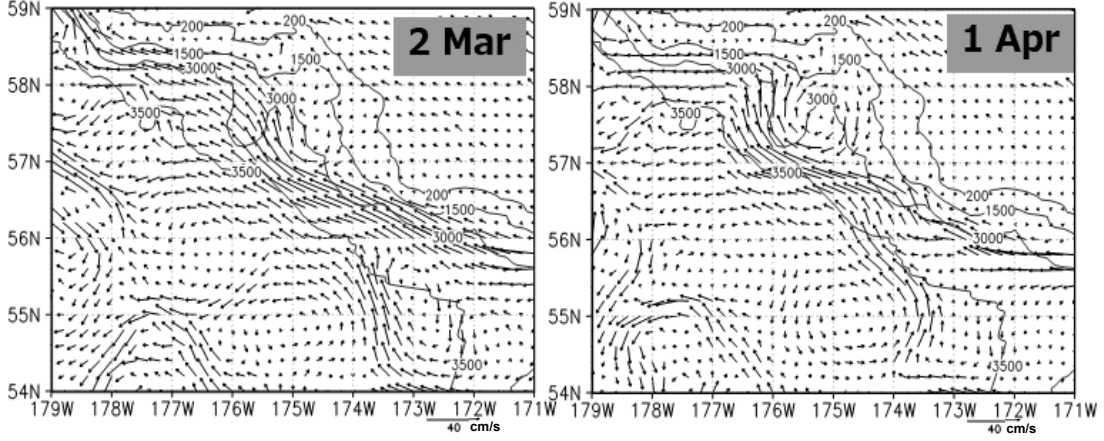
Fig. 6 Evolution of an eddy off the Zhemchug Canyon region. Vector denotes velocity with a unit of cm/s.

4. Eddy generation in shelf-break canyons

We first describe eddy generation processes in the Zhemchug Canyon region (Fig. 6). The BSC flows along the shelf break in mid-February. An anticyclonic eddy starts growing in early March, when the flow is separated from the shelf break in the upstream region of the canyon, because of inertia due to intensification of the BSC. That is, the BSC flows a deep portion of the Zhemchug Canyon. Triggered by this flow separation, the eddy grows to a significant amplitude by early April, and hence, a typical time scale of the eddy growth is of the order of one month. The eddy further grows during spring, thereby pushing the BSC farther off-slope. Since a depth front of 27.0 σθ in mid-March is advected by a barotropic flow, as seen approximately at 57°N, 175°W, the eddy growth and the off-slope movement of the BSC would be caused by baroclinic instability.

Here we examine time scale of the eddy growth in the Zhemchug Canyon seen in Fig. 6 in which a typical time scale of the eddy growth is one month. We use a quasi-geostrophic two-layer model for the upper- and lower-layer stream function ψ_1 and ψ_2, where layer thicknesses are H_1 and H_2, and the along-slope mean flows are U_1 and U_2, respectively. For simplicity, we consider a channel over a β-plane with a typical Coriolis parameter f_0, in which the coastline is rotated by θ from the zonal direction; θ ≈ −45° for the BSC. Then we obtain

$$\left(\frac{\partial}{\partial t} + U_i \frac{\partial}{\partial x}\right) q_i + \frac{dQ_i}{dy} \frac{\partial \psi_i}{\partial x} = 0, \quad (1)$$

where the subscript $i = 1,2$ denotes the upper- and lower-layer variables, and t, x and y denote time, the along-slope and on-slope directions, respectively. q_i and Q_i are perturbed and ambient potential vorticity

$$q_i = \nabla^2 \psi_i - \frac{1}{R_i^2}\left(\psi_i - \psi_j\right), \ i = 1,2, \ j \neq i,$$

$$\frac{dQ_i}{dy} = \left(\beta\cos\theta + (-1)^i \frac{U_s}{R_i^2} + \delta_{2i}\frac{f_0 s}{H_2}\right)y, \ \delta_{2i} = \begin{Bmatrix} 0 \text{ for } i = 1 \\ 1 \text{ for } i = 2 \end{Bmatrix},$$

where s denotes a slope, and $U_s = -(U_1 - U_2)$. Note

that $U_s > 0$ for the BSC since $U_1 < 0$. R_i is a stratification parameter of each layer

$$R_i^2 = \frac{g'H_i}{f_0^2},$$

where g' is the reduced gravity between the two layers. Here, we assume a gentle slope, *i.e.*, $R_1 s \ll H_1 + H_2$, so that the quasi-geostrophic assumption is valid. This assumption is justified by a fact that the BSC in February flows deep part of the Zhemchug Canyon. Assuming a plane wave solution $\psi_i \propto e^{ik(x-ct)}$, where k is the wave number and c is the eigenvalue of the coupled equation (1), we will obtain a growth rate $k\text{Im}(c)$, where $\text{Im}(c)$ is the imaginary part of the eigenvalue.
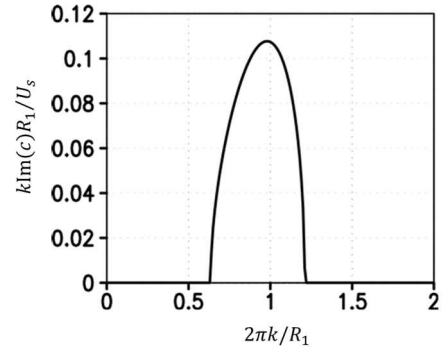

Fig. 7 Scaled growth rate $k\text{Im}(c)U_s/R_1$ vs scaled wavenumber $2\pi R_1/k$.

Figure 7 displays a growth rate for $U_s = 0.05$ ms⁻¹, $H_1 = 800$ m, $H_2 = 2200$ m, $g' = 9.8 \times 7.0 \times 10^{-4}$ ms⁻², $f_0 = 1.2 \times 10^{-4}$ s⁻¹, β = 1.2×10^{-11} s⁻¹m⁻¹ at 57°N. In this case, $R_1 = 1.9 \times 10^4$ m. As for a current with $U_1 = -U_s$ and $U_2 = 0$, then $U_s = 0.05$ms⁻¹ gives an observed transport 4.0 Sv of the BSC (*e.g.* Johnson *et al.*, 2004) if a width of 100 km and a depth of 800 m are assumed. Figure 7 indicates that a scaled maximum growth rate is typically 0.1 at a typical (scaled) wavenumber 1.0. Hence, a time scale for the eddy growth $T = [k\text{Im}(c)]^{-1}$ becomes $T \approx R_1/(0.1U_s) \approx 44$ days at a wave

length $\lambda \approx 2\pi R_1/1.0 \approx 120$ km. These values are consistent with the simulated results (Fig. 6) as well as satellite observations (Ladd, 2012, 2014). This implies that the eddy growth of the seasonal time scale would be caused by baroclinic instability due to potential energy release associated with the main pycnocline.

To examine the energy source of the eddy growth further, the baroclinic energy conversion rate

$$BC = \frac{g}{\rho_0}\overline{\rho' w'}, \quad (2a)$$

and the barotropic energy conversion rate

$$BT = -\overline{u'^2}\frac{\partial \overline{u}}{\partial x} - \overline{u'v'}\left(\frac{\partial \overline{v}}{\partial x} + \frac{\partial \overline{u}}{\partial y}\right) - \overline{v'^2}\frac{\partial \overline{v}}{\partial x}, \quad (2b)$$

(Qiu *et al.*, 2015) were calculated at 200 m. Here, the mean values are defined as the 8-year mean of each month, while the prime denotes deviation from the mean. Since the present simulation is driven by the monthly climatological forcing, the mean values here represent seasonal variations of the BSC and the perturbations represent intra-seasonal variations caused by eddies. The baroclinic energy conversion (equation 2a) occurs along the BSC axis of each month. In February, the region of high conversion rate occurs along the slope where the BSC flows (Fig. 8), consistent with the theoretical results that implies baroclinic instability. The region of the high baroclinic conversion moves off-slope during spring and summer along with the BSC axis propagates off-slope. Intra-seasonal eddies are maintained or even intensified toward summer likely as a result of this continual energy conversion due to baroclinic instability. The barotropic energy conversion rate (equation 2b) is, on the other hand, one order smaller than the baroclinic conversion rate. Therefore, most of EKE stems from the mean potential energy associated with the main pycnocline of the BSC, that is, inclination of the pycnocline toward the slope.

5. Puzzles in the off-slope BSC propagation

What is the mechanism for the westward propagation of the BSC and eddies? We have not succeeded in explaining its mechanism. We first examined whether the westward propagation of annual Rossby waves is possible. The maximum frequency for the baroclinic Rossby wave to exist is

$$\omega_{max} = \frac{1}{2}\beta R_c \quad (3a)$$

where $R_c = c_g/f_0$ is the Rossby radius of deformation in which c_g is the internal gravity wave phase speed. Annual Rossby waves are present if the angular frequency corresponding to one year Ω_{ann} is smaller than ω_{max}. Equation (3a) condition yields

$$\frac{1}{2}\beta R_c > \Omega_{ann}$$

or

$$R_c > 2\Omega_{ann}/\beta \approx 32.0 \text{ km} \quad (3b)$$

to be necessary for the existence of Rossby waves. However, the condition (3b) cannot be satisfied in the Bering Sea because $R_c = c_g/f_0$ is evaluated as 16.4 km based on $c_g = 2.0$ ms^{-1} (*e.g.* Killworth *et al.*, 1997), and hence $R_c < 2\Omega_{ann}/\beta$. That is, the existence condition (3b) is not satisfied with respect to the annual period Rossby waves. In conclusion, the annual signal at the shelf break hardly propagates westward as an annual baroclinic Rossby wave train.
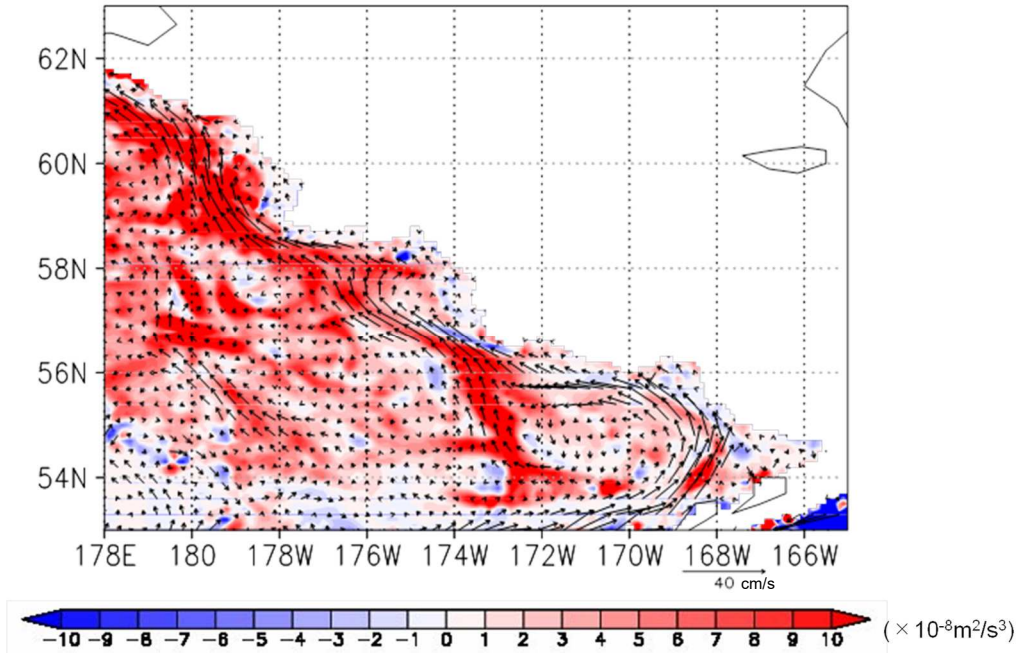

Fig. 8 Color shade depicts the baroclinic energy conversion rate at a depth of 200 m in February along the BSC. Reddish (bluish) color denotes convergence (divergence) of the baroclinic energy. Arrows denote velocity with a unit of cm/s

We also noticed that the propagation of long Rossby waves does not give the answer neither; $c_g = 2.0$ ms^{-1} (*e.g.* Killworth *et al.*, 1997) implies an estimation of the phase speed of the long baroclinic Rossby wave $c_R = -\beta c_g{}^2 f_0{}^{-2}$ to be -0.3×10^{-2} ms^{-1} for $f_0 = 1.2 \times 10^{-4}$ s^{-1}, and $\beta = 1.2 \times 10^{-11}$ s^{-1}m^{-1} at 57°N. The offshore propagation speed in the numerical models is 1.3×10^{-2} ms^{-1} (see Fig. 3), which is faster than the long Rossby waves' estimation. The analyses above suggest that the linear wave theory would not be appropriate for the westward propagation of waves/eddies. Nonlinearity should be taken into account. We are seeking its proper mechanism.

6. Conclusion and discussion

Seasonal variations of the Bering Slope Current (BSC) and eddies were discussed by analyzing an OGCM output. The model output simulates the seasonal variations of the BSC realistically; the BSC flows along the shelf break over the slope in winter, and moves off-slope during spring and summer. Eddies start growing in winter in the shelf-break canyons and cause the BSC's separation from the shelf-break. The eddies obtain kinetic energy converted from potential energy associated with deepening of the main pycnocline of the BSC. The growth rate of the eddies is the order of 1 month. A linear baroclinic instability theory with a sloping bottom can explain this slow growth.

Offslope propagation of the BSC, observed by satellites as well as simulated by the OGCM, is still puzzling. An annual baroclinic Rossby wave is not able to exist because their maximum frequency ω_{max} is smaller than the frequency associated with the annual oscillation. Further, a linear long wave is far slow compared with the propagation speed of the observed and simulated westward propagation. Therefore, the linear theories are not appropriate for the BSC's offslope propagation in the OGCM as well as in reality; nonlinear effects would be important.

The seasonal variation of the BSC is correlated with the deepening of isopycnal levels adjacent to the slope in winter (see Fig. 4). Thus, it is important to understand the mechanism of the wintertime isopycnal deepening to elucidate the BSC's seasonality. One hypothesis is a remote effect of wind forcing in the Gulf of Alaska; the BSC's deepening is apparently correlated with pycnocline deepening along the coast of Gulf of Alaska, which is likely caused by intensified wind stress due to the Aleutian Low. The isopycnal depth anomaly along the shelf break in the Bering Sea can be traced back to the Alaskan Stream via the Aleutian Islands (Fig. 9). Coastally trapped waves may be an agent to link the anomaly between the Gulf of Alaska and the Bering Slope. The study is now underway.
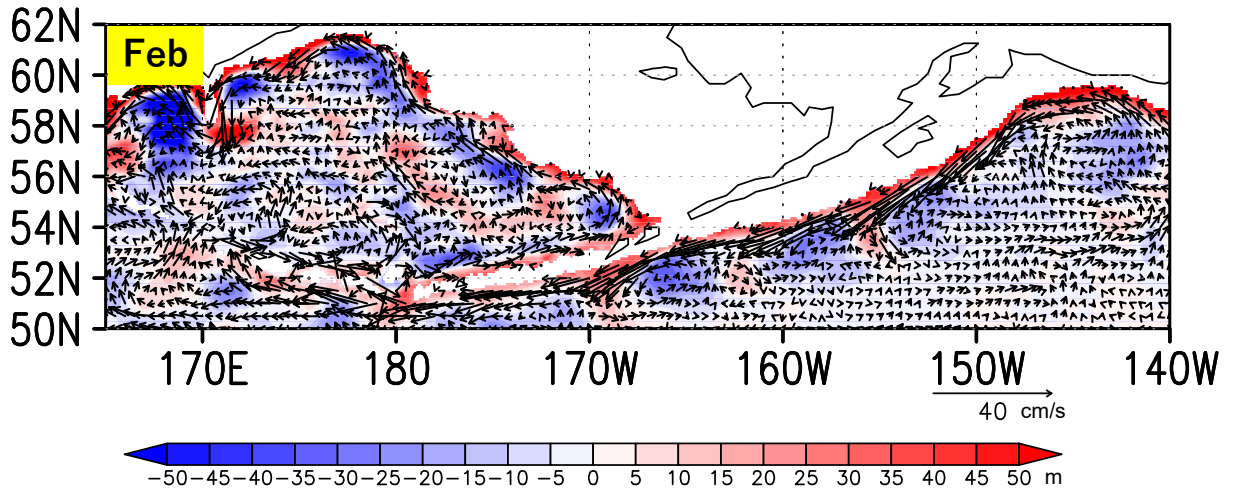

Fig. 9 Isopycnal depth anomaly of 27.0 σ$_\theta$ (color shades with a unit of m) in February. Reddish color denotes deepening, while bluish color denotes shoaling. Vectors indicate velocity at 27.0 σ$_\theta$ isopycnal surface with a unit of cm/s.

References
Foreman, M.G.G., P. F. Cummins, J. Y. Cherniawsky, and P. Stabeno (2006): Tidal energy in the Bering Sea. *J. Mar. Res.*, **64**, 797-818.

Johnson, G.C., Stabeno, P.J., Riser, S.C. (2004): The Bering Slope Current system revisited. *J.Phys. Oceanogr.*, **34**, 384-398.

Killworth, P.D., D.B. Chelton, and R.A. de Soeke (1997): The speed of observed and theoretical long extratropical planetary waves. *J.Phys. Oceanogr.,* **27**, 1946-1966.

Ladd, C., Stabeno, P.J., O'Hern, J.E. (2012): Observations of a Pribilof eddy. *Deep-Sea Res. I.*,66, 67-76.

Ladd, C. (2014): Seasonal and interannual variability of the Bering Slope Current. *Deep-Sea Res.II.*, **109**, 5-13.

Matsuda, J., H. Mitsudera, T. Nakamura, Y. Sasajima, H. Hasumi, and M. Wakatsuchi. (2015): Overturning circulation that ventilates the intermediate layer of the Sea of Okhotsk and the North Pacific: The role of salinity advection. *J. Geophys. Res.-Oceans.*, **120**, 1462-1489

Mizobata, K. and 8 co-authors (2002): Bering Sea cyclonic and anticyclonic eddies observed during summer 2000 and 2001. *Prog. in Oceanogr.*, **55**, 65–75.

Noh Y, & Jin Kim H. (1999): Simulations of temperature and turbulence structure of the oceanic boundary layer with the improved near‐surface process. *J. Geophys. Res. Oceans*, **104,** 15621-15634.

Okkonen,S.R. (2001): Altimeter observations of the Bering Slope Current eddy field. *J. Geophys. Res*, **106**, 2465-2476

Qiu, B., S. Chen, D.L. Rudnick, and Y. Kashino (2015): A new paradigm for the North Pacific subthermocline low-latitude western boundary current system. *J.Phys. Oceanogr.,* **45**, 2407-2423.

Pickart, R.S., G.W.K. Moore, A.M. Macdonald, I.A. Renfrew, J.E. Walsh, and W.S. Kessler (2009): Seasonal evolution of Aleutian low-pressure systems: Impactions for the North Pacific sub-polar circulation. *J.Phys. Oceanogr.*, **39**, 1316-1339.

Springer, A. M, McRoy, C. P., Flint, M. V (1996): The Bering Sea Green Belt: shelf-edge processes and ecosystem production. Fisheries Oceanography, 5(1996), pp. 205-223.

Tanaka, T., I. Yasuda, K. Kuma, J. Nishioka (2017): Evaluation of the biogeochemical impact of iron-rich shelf water to the Green Belt in the southeastern Bering Sea. *Continental Shelf Res.*, **143**, 130-138.

Summary in Japanese
和文要約

ベーリングスロープカレントの季節変動

三寺史夫[1]、平野洋一[2]、西川はつみ[3]、周宏瑋[4]

[1]北海道大学低温科学研究所, [2]北海道大学環境科学院
[3]東京大学大気海洋研究所, [4]水産研究・教育機構

　ベーリングスロープカレント（BSC）の季節変動をモデルのアウトプットを用いて調べた。傾圧不安定によって渦が生じ、それに伴い BSC が大陸棚から離れて沖向きに進んだ。冬季における BSC 表層流の強化が渦形成の原因である。その強化はアラスカンストリームの強化と対応しており、アラスカ湾からの遠隔影響であろうと考えられる。

Correspondence to: H. Mitsudera,
humiom@lowtem.hokudai.ac.jp